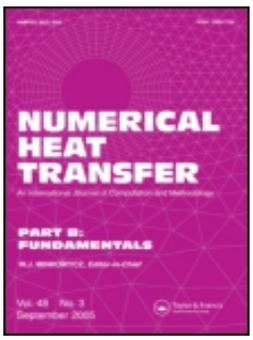

Taylor & Francis
Taylor & Francis Group

Numerical Heat Transfer, Part B: Fundamentals
An International Journal of Computation and Methodology

ISSN: 1040-7790 (Print) 1521-0626 (Online) Journal homepage: https://www.tandfonline.com/loi/unhb20

Modeling of Heat Transfer Across the Interface in Two-Fluid Flows

Yeng-Yung Tsui , Shi-Wen Lin & Kuen-Je Ding

To cite this article: Yeng-Yung Tsui , Shi-Wen Lin & Kuen-Je Ding (2014) Modeling of Heat Transfer Across the Interface in Two-Fluid Flows, Numerical Heat Transfer, Part B: Fundamentals, 66:2, 162-180, DOI: 10.1080/10407790.2014.894450

To link to this article: https://doi.org/10.1080/10407790.2014.894450

Numerical Heat Transfer, Part B, 66: 162–180, 2014

ISSN: 1040-7790 print/1521-0626 online
DOI: 10.1080/10407790.2014.894450

Taylor & Francis
Taylor & Francis Group

MODELING OF HEAT TRANSFER ACROSS THE INTERFACE IN TWO-FLUID FLOWS

Yeng-Yung Tsui, Shi-Wen Lin, and Kuen-Je Ding
Department of Mechanical Engineering, National Chiao Tung University, Hsinchu, Taiwan, Republic of China

A model is presented in this article to deal with heat transfer across the interface separating two immiscible fluids. It is suitable to be incorporated into interface-tracking methods, such as volume-of-fluid (VOF) methods, because a sharp interface is available in these approaches. The temperature at the interface and the heat flux through it are calculated in such a way that the continuity of the two properties at the contact surface is satisfied explicitly. With use of these values, the temperature either at the centroid or on a face of the interface cell can be estimated, which serves as Dirichlet boundary condition for the energy equation. The temperature field is then calculated by solving the energy equations for the two fluids simultaneously in an implicit way. This method is first assessed via testing on two heat conduction problems in which two solids are in contact. Good agreement between numerical solutions and theory is obtained. To demonstrate its capability, it is applied to two kinds of heat transfer problems, one being the collapse of a heated water column in a cavity, and the other the falling of a molten tin droplet in an oil tank. The effect of fluid flow on the heat transfer is clearly illustrated.

INTRODUCTION

Free surface flow with heat transfer can be found in many industrial applications. As examples, injection of gas into molten metal has been a common method for the molten metal refining process in refining and casting plants [1]. In direct-contact heat exchangers, liquid or gas is bubbled through another liquid [2]. In the filling process of mold casting, the fluid and accompanying heat transfer are closely related to the casting quality, surface finish and segregation of the cast part, and mold erosion [3, 4]. Injection-molded parts suffer from shrinkage and warpage after injection. In order to simulate the deformation, residual stresses induced by temperature during the molding process must be calculated [5].

In two-fluid flows, the surface boundary separating the two fluids undergoes continuous distortion, which may cause overturning or breaking of the surface or coalescence of two such surfaces. A popular approach to tackle these problems is

Received 25 November 2013; accepted 27 December 2013.

Address correspondence to Yeng-Yung Tsui, Department of Mechanical Engineering, National Chiao Tung University, 1001 Ta-Itsueh Road, Hsinchu 300, Taiwan, Republic of China. E-mail: yytsui@mail.nctu.edu.tw

Color versions of one or more of the figures in the article can be found online at www.tandfonline.com/unhb.

NOMENCLATURE

C_p	specific heat	$\gamma(r)$	flux limiter depending on gradient ratio
f	VOF function	$\vec{\delta}$	distance vector
F^d	diffusive flux	μ	viscosity
$\vec{g}$	gravitational acceleration	ρ	density
h	specific energy	σ	surface tension coefficient
k	thermal conductivity	$\tilde{\tilde{\tau}}$	viscous stresses
Δn	normal distance away from the interface	Subscripts	
P	pressure	D	downstream cell
$\dot{q}$	heat flux	f	cell face
r	gradient ratio	fj	jth cell face
$\vec{s}_f^w$	surface vector of wetted area	int	interface
$\vec{S}_f$	surface vector	N	neighboring cell
$\vec{S}$	source terms in momentum equation	P	primary cell
t	time	U	upstream cell
Δt	time-step size	UU	far upstream cell
T	temperature	1, 2	fluids 1 and 2
Δv	cell volume	Superscripts	
$\vec{V}$	velocity vector	n	new time step
α	thermal diffusivity	o	old time step

to use a Euler mesh and allow the interface to move around in the mesh. Two indicator functions, volume-of-fluid (VOF) and level set functions, are usually adopted to track and locate the interface [6–10]. The entire flow field is solved in the manner that the different fluids are treated as one fluid with variable thermophysical properties. However, owing to the abrupt change of material properties across the interface, numerical calculations often suffer instability problems. A common approach to relieve this is to diffuse the interface so that the gradients of the properties are smeared. This smoothing practice is usually adopted in solving the Navier-Stokes equations with free surface flows [11, 12]. Application of the diffused-interface method for the energy equation may result in significant errors in calculating temperature gradients around the interface.

As reported by Storr and Behnia [13] for a heated falling jet, unrealistic temperature distributions appear in their results; large temperatures are presented as hot-spots at the back edge of the jet. To prevent unrealistic temperature distribution, Pericleous et al. [14] simply employed the second-order total variation diminishing (TVD) scheme of van Leer [15] for calculation of velocity and temperature. The accuracy of this simple way is questionable because diffuseness of the interface cannot be avoided, as evidenced in their results. Mehdi-Nejad et al. [16] showed that the van Leer scheme alone is not sufficient to eliminate false diffusion, especially if the differences in thermal properties between the two fluids are large. To remedy this defect, a ''two-temperature model'' was used in the interface cells in their study. This two-temperature model is similar to the method employed by Davidson and Rudman [17]. The interface is first reconstructed using the VOF function to separate the interface cell into two parts occupied by the two fluids individually. The total convective energy flux crossing the cell face is obtained

via combination of the two individual fluid fluxes. For the cells away from the interface, the flux-corrected transport algorithm of Zalesak [18] is used by Davidson and Rudman. Discretization of the diffusive flux in their study is based on an analysis of 1-D diffusion across the interface.

Accompanied by heat transfer, mass transfer is also included in such processes as boiling and evaporation. In simulating these flows, the temperature at the interface is often assumed to be known at the saturated temperature [19–21]. In contrast, the temperature at the interface is not known *a priori* in the flow without phase change. Care must be taken in calculating heat transfer in the region near the interface. In this study, a new approach is proposed to account for the heat transfer across the fluid interface without phase change involved. In this method, the temperature of the interface is obtained from the continuity condition for the temperature and diffusive heat flux. With use of this temperature as an internal boundary condition, the temperature field for the two fluids can be solved without suffering from any numerical diffusion at all.

MATHEMATICAL MODEL

The flows in both fluids are assumed to be laminar and incompressible. The conservation equations for the two fluids can be given by one set of equations.

$$\nabla \cdot \vec{V} = 0 \tag{1}$$

$$\frac{\partial \rho \vec{V}}{\partial t} + \nabla \cdot (\rho \vec{V} \otimes \vec{V}) = -\nabla P + \nabla \cdot \tilde{\tilde{\tau}} + \rho \vec{g} + \vec{S} \tag{2}$$

$$\frac{\partial \rho h}{\partial t} + \nabla \cdot (\rho \vec{V} h) = \nabla \cdot \left(\frac{k}{C_p} \nabla h \right) \tag{3}$$

where $\vec{V}$ is the velocity, ρ the density, h the specific energy, P the pressure, k the thermal conductivity, C_p the specific heat, and $\tilde{\tilde{\tau}}$ the viscous stress. The momentum source $\vec{S}$ is generally zero except in the cells containing the interface, where surface tension acts. With the CSF (continuum surface force) model [22], the surface tension can be formulated as a body force.

$$\vec{S} = -\sigma \nabla \cdot \left(\frac{\nabla f}{|\nabla f|} \right) \nabla f \tag{4}$$

where f is the VOF function and σ is the surface tension coefficient.

Within the frame of the VOF method, the interface is determined from the volume fraction f. It is either 0 or 1 in the single-phase cells and a value greater than 0 and less than 1 in the cells containing the interface. The transport equation for this function can be cast as

$$\frac{\partial f}{\partial t} + \nabla \cdot (\vec{V} f) = 0 \tag{5}$$

NUMERICAL METHODS

Numerical Methods for Interface Tracking

An interface-tracking procedure, termed CISIT, has been developed by the present authors recently [23]. Unlike other VOF methods, the interface is simply characterized by the contour surface of VOF value 0.5, which can easily be reconstructed. The moving of the interface through the grid is fulfilled by enforcing mass conservation of the fluids across the control surface of the interface cells in a predictor-corrector manner. This procedure is briefly addressed in the following. Details about the method can be found in the original article.

To obtain the contour surface (or contour line in 2-D problems, as exemplified in the present study), a linear interpolation practice is employed. The original VOF value is stored at the centroid of each grid cell. An interpolation practice is first carried out to obtain this function on the grid nodes. It is followed by examining the two end nodes of each side edge of the grid cell. The edge is intersected by the interface when the VOF value of one node is less than 0.5 and the other greater than 0.5. A continuous piecewise linear interface can then be built after this process proceeds throughout all the grid cells.

To illustrate the moving of the interface, an interface cell shown in Figure 1 is under consideration. The surface area wetted by one of the fluids on the face of its control surface is denoted by $\vec{s}_f^w$. This fluid flows into or out of the cell through this wetted surface. Thus, the mass conservation of the fluid in this cell gives rise to the following equation:

$$\frac{\Delta v}{\Delta t}(f_{\mathrm{P}}^n - f_{\mathrm{P}}^o) + \sum_j \vec{V}_{fj} \cdot \vec{s}_{fj}^w = 0 \tag{6}$$

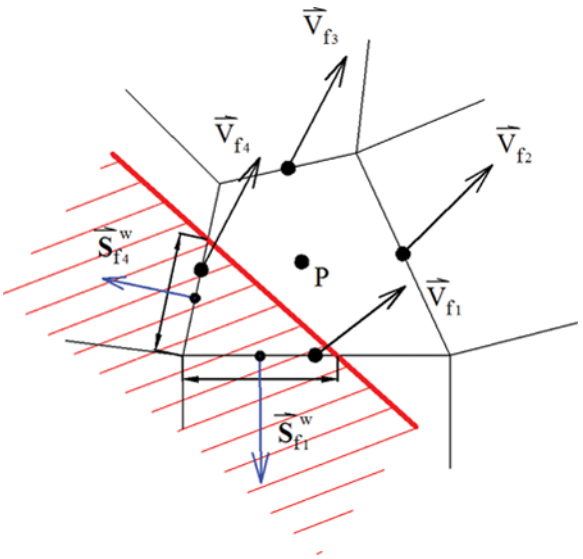

Figure 1. Illustration of the wetted area for an interface cell.

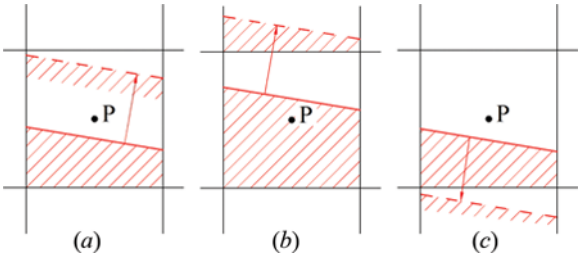

Figure 2. Illustration of the interface motion in a cell: (*a*) normal filling; (*b*) overfilling; (*c*) overdraining.

where the index j indicates the jth face of the control surface and the sum is over all the faces. It gives a new VOF value f_P^n for the interface cell. This calculation performs well when the interface remains in the cell during the time marching (see Figure 2*a*). However, it cannot tackle the situation that arises when the interface is moving to the adjacent cell in the time interval. Four situations need to be considered: overfilling ($f_P^n > 1$), underfilling ($f_P^n < 1$), overdepleting ($f_P^n < 0$), and underdepleting ($f_P^n > 0$). Consider an example that a vessel is filled with water. When water is flowing into the vessel, the value f_P^n will be greater than 1 (i.e., the vessel is overfilled) as the time interval Δt is large enough (see Figure 2*b*). Similarly, the VOF will become less than 0 as the vessel is overdrained (see Figure 2*c*). For the overfilling case the excessive portion of fluid must be reallocated to the neighboring cells at the downstream, whereas the overdrained fluid in the overdepleting case must be retrieved from the downstream cells. These overfilling and overdepleting situations occur when the velocity field is considerably uniform. In highly shear flows, f_P^n may remain to be less than 1 (underfilling) or greater than 0 (underdepleting) when the interface is advancing or retreating to the neighboring cell. For underfilling, fluid must be retrieved from the downstream cells to fill the considered cell such that f_P^n is equal to 1. As for the case of underdepleting, the residual fluid in the cell must be allocated to the downstream cells so that f_P^n becomes zero.

Numerical Methods for Velocity Field

The governing equations for the flow field are discretized using the finite-volume method, suitable for unstructured grids [24]. The diffusive flux through the face of a control volume is given by

$$F^d = \frac{\mu S_f^2}{\vec{\delta}_{PN} \cdot \vec{S}_f}(\phi_N - \phi_P) + \mu(\nabla\phi)_f \cdot \left(\vec{S}_f - \frac{S_f^2}{\vec{\delta}_{PN} \cdot \vec{S}_f}\vec{\delta}_{PN}\right) \tag{7}$$

where $\vec{S}_f$ is the surface vector of the face, the subscripts P and N denote the centroids of the considered cell and its neighboring cell common to the face, and $\vec{\delta}_{PN}$ is the vector connecting P and N.

As for convection, the face flux value is approximated by

$$\phi_f = \phi_U + \frac{\gamma(r)}{2}(\phi_D - \phi_U)$$

where the subscripts U and D denote the cells upstream and downstream of the considered face, respectively, and γ represents flux limiter, which is a function of the gradient ratio r defined as

$$r = \frac{\phi_U - \phi_{UU}}{\phi_D - \phi_U} \tag{8}$$

Here ϕ_{UU} is the value at a node far upstream, estimated by

$$\phi_{UU} = \phi_D - 2(\nabla\phi)_U \cdot \vec{\delta}_{UD} \tag{9}$$

A variety of TVD and NVD schemes are available by assigning different expressions to the flux limiter function $\gamma(r)$ [25]. In the following calculations, the van Leer scheme is employed, which is given by

$$\gamma(r) = \frac{r + |r|}{r + 1} \tag{10}$$

In solving the Navier-Stokes equations, the large gradients in density and viscosity across the interface may cause solution oscillation and numerical instability. In order to relieve this problem, these properties are artificially diffused in the region of the interface. They are calculated from a smoothed VOF function f^* as

$$\rho^* = f^*\rho_1 + (1 - f^*)\rho_2 \tag{11a}$$

$$\mu^* = f^*\mu_1 + (1 - f^*)\mu_2 \tag{11b}$$

An averaging smoother is used to smear the VOF function. The original f is stored at the cell centroid. An interpolation practice is carried out to find VOF on the grid nodes (vertices). Then, a new VOF at the centroid (f^*) is obtained by averaging over those values on all the cell vertices. It is usual to take two such smoothing steps in the calculation to enhance the smearing effect.

The coupling between momentum and continuity equations is tackled using a noniterative predictor-corrector algorithm. The momentum equations are solved first. The resulting velocities need to be adjusted and the prevailing pressure must be updated such that the continuity equation is satisfied. The enforcement of mass conservation results in a pressure-correction equation. After this equation is solved, the velocities and pressure are upgraded according to the pressure corrections. Two correction steps are usually taken. More information about this algorithm can be found in the study [26].

Numerical Methods for Temperature Field

The energy equation is discretized in a similar way to the momentum equation; Eq. (7) is adopted for approximation to the energy diffusion and the van Leer scheme for the energy convection. However, it needs to be stressed that with use of the diffused-interface technique described in the above in solving the energy equation in the interface region would distort the heat transfer rate there and, thus,

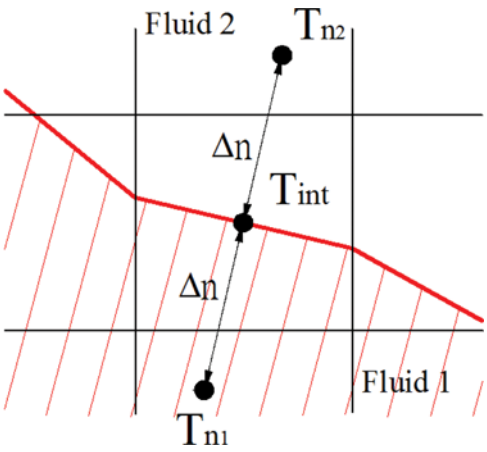

Figure 3. Illustration for calculating temperature gradients at interface.

bring about considerable inaccuracy in temperature distribution. A sharp-interface method is introduced below.

In the heat transfer process, both temperature and heat flux are continuous at the contact boundary between the two fluids.

$$T_{\text{int}} = T_1^+ = T_2^- \tag{12}$$

$$\dot{q}_{\text{int}} = -k_1 \left(\frac{\partial T_1}{\partial n}\right)^+ = -k_2 \left(\frac{\partial T_2}{\partial n}\right)^- \tag{13}$$

Using one-sided differencing, the heat fluxes on the two sides of this contact surface can be approximated as

$$k_1 \frac{T_{n1} - T_{\text{int}}}{\Delta n} = k_2 \frac{T_{\text{int}} - T_{n2}}{\Delta n} \tag{14}$$

where, as seen in Figure 3, T_{n1} and T_{n2} denote the temperatures at a normal distance Δn away from the interface for the two separate fluids, which can be obtained by interpolation from surrounding nodal values. The interface temperature can be found as

$$T_{\text{int}} = \frac{k_1 T_{n1} + k_2 T_{n2}}{k_1 + k_2} \tag{15}$$

The temperature gradients on the two sides of the interface can then be obtained. The interface is regarded as an internal boundary for the temperature field. The temperature and heat flux obtained must be imposed as boundary conditions. For the cells next to the interface cell to see proper such boundary conditions, an approximation practice is conducted to find the temperature at relevant points using the interface temperature and heat flux. As an illustration, the temperature field in fluid 1 is under consideration. It is shown in Figure 4 that two situations need to be considered.

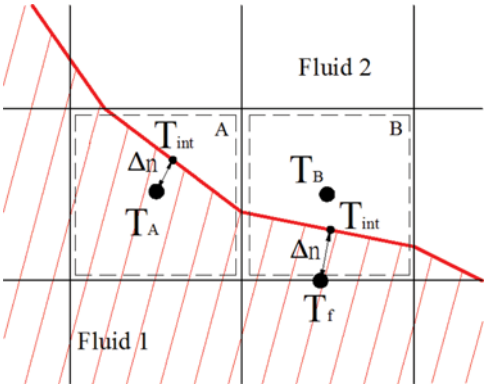

Figure 4. Illustration for calculating temperatures at the centroid and a face of the interface cell.

The centroid of the interface cell A is located in the region of fluid 1. The temperature at this point can be calculated by

$$T_A = T_{\text{int}} + \left(\frac{\partial T_1}{\partial n}\right)\Delta n \tag{16}$$

In the second situation, the centroid of the interface cell B lies in the region of the other fluid. For the neighboring cell on the south, the face temperature T_f is required to be known, which can be estimated in a similar way as Eq. (16). The centroid temperature T_A and the face temperature T_f form Dirichlet boundary conditions for fluid 1. The same treatments can be conducted for the other fluid. As in cell B, the temperature T_B at the centroid is calculated to give boundary condition for fluid 2.

The discretized energy equation is solved in an implicit manner, which can be cast into the following form:

$$A_P T_P = \sum A_C T_C + S \tag{17}$$

where the subscript C denotes the surrounding cells. In order to treat the two individual fluid fields as a whole, the temperature distribution in the interface cells, which has been obtained as T_P^* using the method just described, is also expressed in the above form with the following settings:

$$A_P = D \quad A_C = 0 \quad S = DT_P^* \tag{18}$$

where D is a large number.

RESULTS AND DISCUSSION

The solution method is first tested on one-dimensional model problems for which theoretical or reference solutions are available. Realistic problems under

consideration include collapsing water flow in a cavity and falling of a liquid tin droplet in an oil tank.

1-D Conduction in Two Solids with Continuous Initial Temperature

The heat transfer in a finite solid block and a semi-infinite block is considered. The configuration of this test problem is shown in Figure 5. The first block has a length L_1 (1 m) and the other one has a much longer length L_2 (20 m). The two solid blocks are in perfect contact at $x=0$. The contact resistance is ignored and, thus, the continuity condition of Eqs. (12) and (13) is applied at this contact surface. Both blocks have the same initial temperature T_0 ($=300$ K). A high temperature T_B (400 K) is imposed at the left boundary of block 1. This problem can be solved using Laplace transforms and contour integration in the complex domain [27] to yield

$$\frac{\theta_1}{\theta_B} = 1 - \frac{2\varepsilon}{\pi}\int_0^\infty \frac{\sin\xi(x+L_1)}{\cos^2(\xi L_1)+\varepsilon^2\sin^2(\xi L_1)}\exp(-\alpha_1 t\xi^2)\frac{d\xi}{\xi} \tag{19}$$

$$\frac{\theta_2}{\theta_B} = 1 - \frac{2}{\pi}\int_0^\infty \left[\frac{\cos(\xi L_1)\sin(\eta\xi x)+\varepsilon\sin(\xi L_1)\cos(\eta\xi x)}{\cos^2(\xi L_1)+\varepsilon^2\sin^2(\xi L_1)}\right]\exp(-\alpha_1 t\xi^2)\frac{d\xi}{\xi} \tag{20}$$

where $\theta = T - T_0$, $\eta = \sqrt{\alpha_1/\alpha_2}$, $\varepsilon = \eta k_2/k_1$, $\xi = \sqrt{r/\alpha_1}$, and r is the radius in the complex plane. The interface temperature is that at $x=0$. Numerical integration of the above equations is carried out to find the temperature distribution.

The thermal diffusivities and conductivities are given by $\alpha_1 = 0.1$, $\alpha_2 = 0.01$, and $k_1 = k_2 = 1$. The grid size used in calculations is $\Delta x = 0.02$ m. The time variation of the interface temperature is shown in Figure 6*a* and the temperature distribution at various instants is given in Figure 6*b*. It is obvious that the agreement between numerical calculations and theoretical solutions is very good, which validates the method to treat the heat transfer at contact surface.

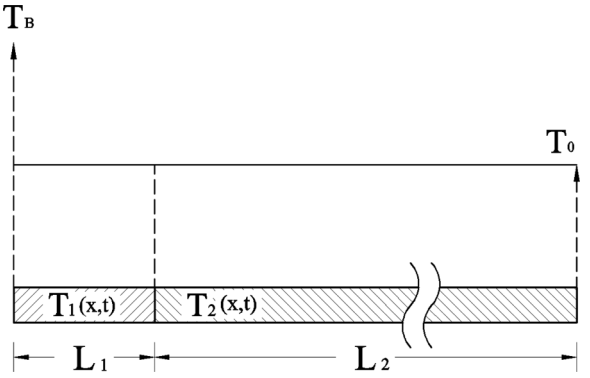

Figure 5. Illustration for the 1-D problem with a finite solid and a semi-infinite solid.

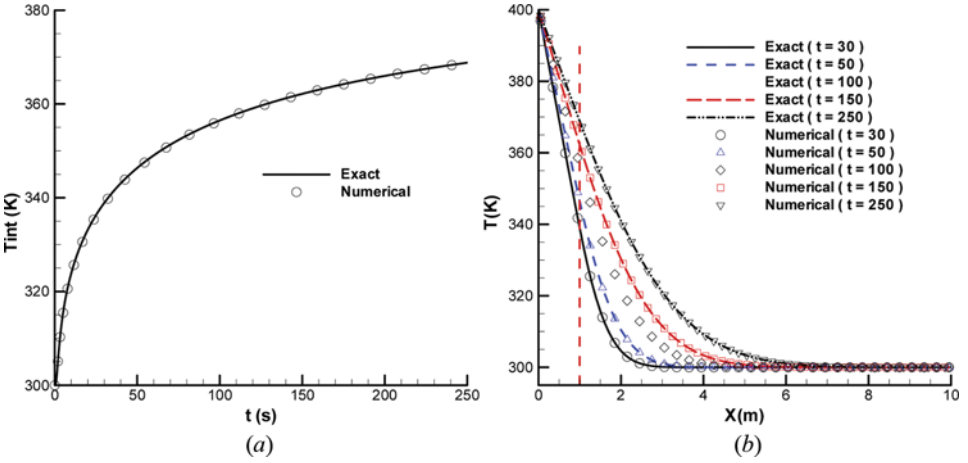

Figure 6. 1-D conduction with a finite and a semi-infinite solid: (*a*) variation of interface temperature; (*b*) temperature distribution at various times.

1-D Conduction in Two Solids with Discontinuous Initial Temperature

In this problem, the two solid blocks in contact are of the same finite length L (5 m). As illustrated in Figure 7, temperature is uniformly distributed initially in the blocks, but different from each other. The initial temperature is T_{B1} (400 K) for block 1 and T_{B2} (300 K) for block 2. The temperatures at the two outer boundaries remain the same as their initial values during the heat transfer process. To our best knowledge, there is no theoretical solution to this problem because the continuity of temperature at the internal boundary of contact surface is not satisfied. However, a reference solution is derived in the following way.

First, consider heat conduction in a 1-D solid of length L, whose surfaces at $x = 0$ and $x = L$ are maintained at constant temperatures T_C and T_D. The temperature is uniformly distributed at T_0 initially. With use of the superposition principle and

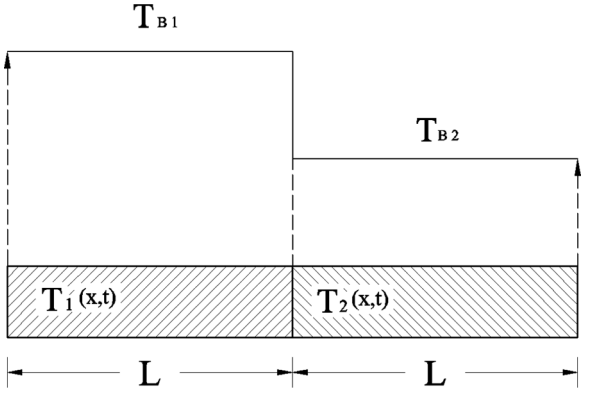

Figure 7. Illustration for the 1-D problem with two finite solids.

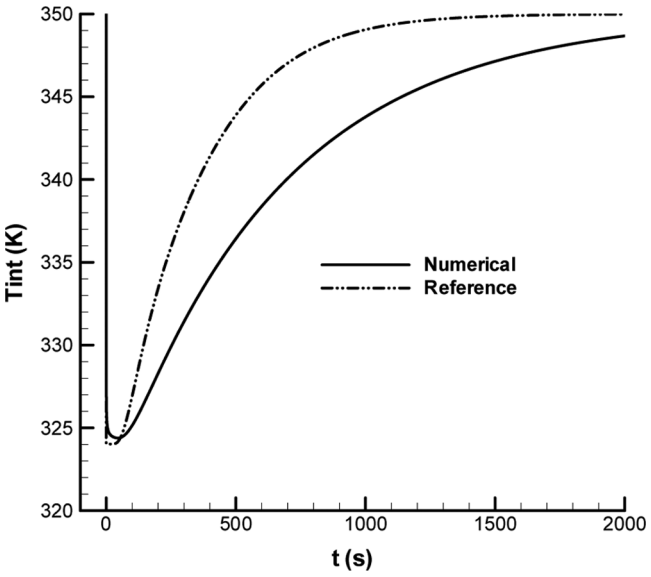

Figure 8. Variation of interface temperature for 1-D conduction with finite solids.

the method of separating variables, the solution can be found as

$$T = T_C + (T_D - T_C)\frac{x}{L} + \sum_{n=1}^{\infty}\left\{\frac{2}{n\pi}[(T_D - T_0)(-1)^n + (T_0 - T_C)]\sin\left(\frac{n\pi x}{L}\right)\exp\left[-\alpha t\left(\frac{n\pi}{L}\right)^2\right]\right\} \quad (21)$$

For the problem of two solid blocks the temperature at the contact surface is assumed to be $T_{\text{int,ref}}$. Thus, the temperature distribution in the two blocks is of

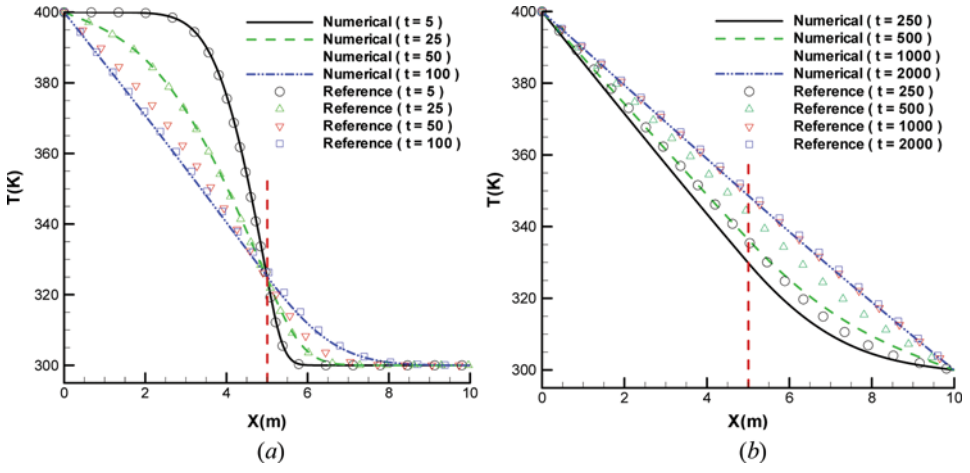

Figure 9. Temperature distribution at various times for 1-D conduction with finite solids.

a form similar to the above by using $T_{\text{int,ref}}$ as a boundary temperature. Applying the continuity condition for heat flux at the contact surface [Eq. (13)] gives the interface temperature.

$$T_{\text{int,ref}} = \frac{\frac{k_1}{k_2} T_{B1} + T_{B2} + 2\sum_{n=1}^{\infty} \left\{ T_{B2} \exp\left[-\alpha_2 t\left(\frac{n\pi}{L}\right)^2\right] + \frac{k_1 T_{B1}}{k_2} \exp\left[-\alpha_1 t\left(\frac{n\pi}{L}\right)^2\right] \right\}}{\frac{k_1}{k_2} + 1 + 2\sum_{n=1}^{\infty} \left\{ \exp\left[-\alpha_2 t\left(\frac{n\pi}{L}\right)^2\right] + \frac{k_1}{k_2} \exp\left[-\alpha_1 t\left(\frac{n\pi}{L}\right)^2\right] \right\}} \tag{22}$$

Initial temperature at the interface can be obtained as

$$T_{\text{int,ref}}(t=0) = \frac{k_1 T_{B1} + k_2 T_{B2}}{k_1 + k_2} \tag{23}$$

When time approaches infinity, the interface temperature is the same as its initial value.

$$T_{\text{int,ref}}(t \to \infty) = T_{\text{int,ref}}(t=0) \tag{24}$$

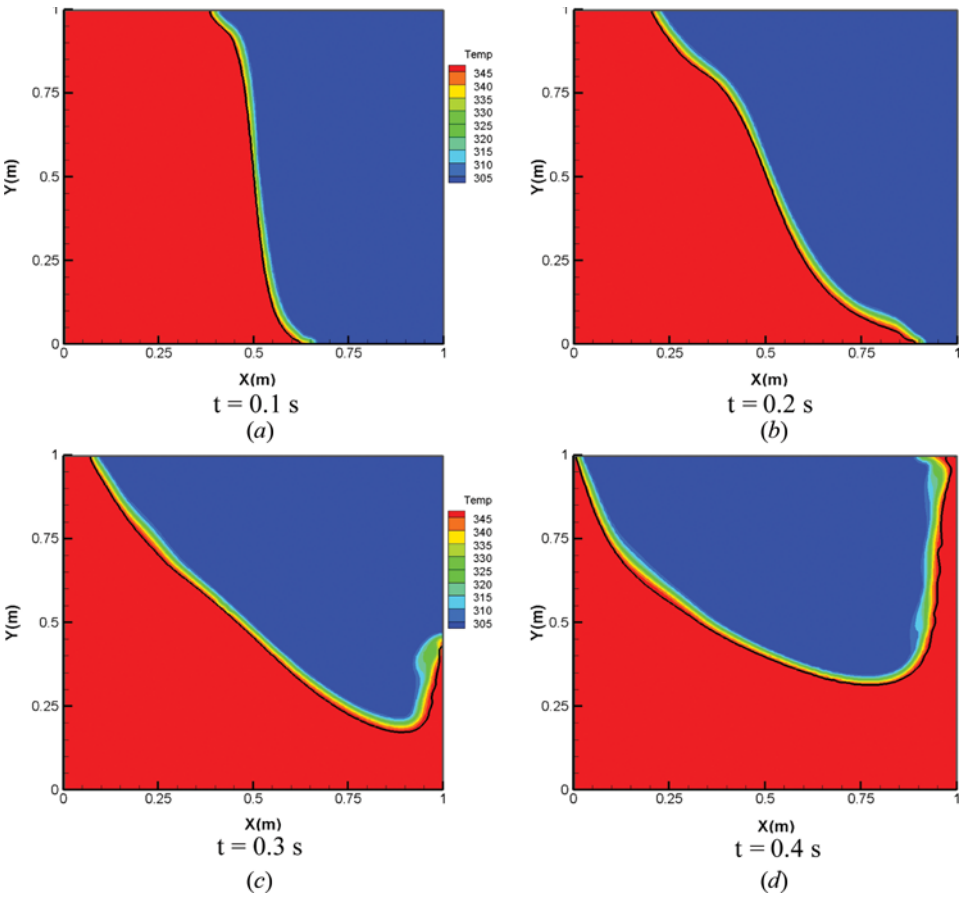

Figure 10. Temperature distribution at various times for collapsing flow.

The same thermal properties as the first model problem are used in simulations. The calculated results are given in Figures 8 and 9. Both the initial interface temperature and that at steady state are 350 K according to the above solution. It is interesting to see from Figure 8 that the interface temperature drops very sharply from its initial value, followed by gradual recovery and then approaching the steady state. It can be found that both the numerical and reference solutions have very similar trends. However, the recovery in the reference solution is faster, leading to a higher level of interface temperature. The above observation is also reflected in the temperature distribution shown in Figure 9. As seen in Figure 9*a* for time smaller than 100 s, the temperature curves intersect at about 325 K, which corresponds to the interface temperature. The numerical solution is close to the reference solution at this stage. Considerable disagreement is detected between the two in later time given in Figure 9*b*, corresponding to the recovery stage seen in Figure 8. The problem approaches the steady state at large time and the disagreement gradually dwindles. It needs to be stressed that the reference solution given above is not exact. It is used only for quantitative assessment of the numerical method, not to evaluate the accuracy of the method.

Collapsing Flow in a Cavity

A square cavity of 1 m is divided into two equal vertical sections. The left part is filled with water of 350 K and the right contains air at 300 K. The surrounding walls are assumed to be insulated. The grid size used in calculations is 0.01 m.

The evolution of the interface and the temperature distribution are presented in Figure 10. Collapse of the water column on the left side causes a water front to move along the bottom wall toward the right and, in the meanwhile, a water front on the top to retreat toward the left. After the front on the bottom reaches the right-hand side

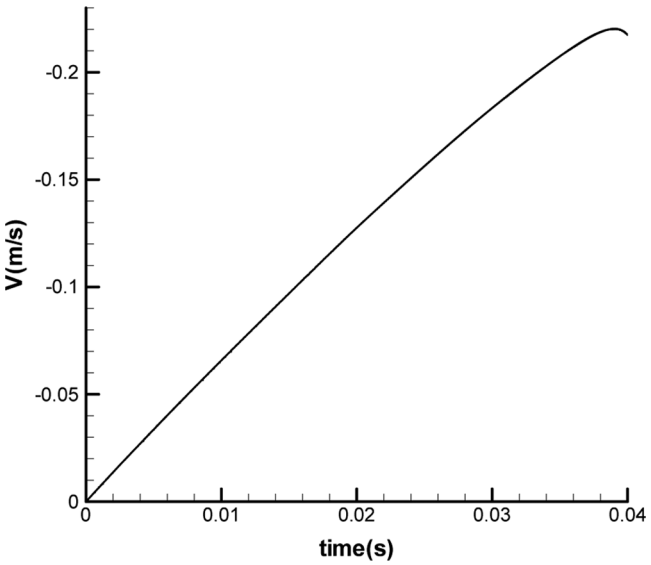

Figure 11. Variation of droplet speed for the case with zero initial velocity.

wall, it moves upward along this wall. The heat transfer mechanism is mainly controlled by the diffusion. It can be detected that the thermal diffusion process mainly occurs on the air side, because the thermal diffusivity of air is an order higher than that of water. The thermal layer around the interface remains thin during the process. This is not unexpected, because the thermal penetration of heat conduction is proportional to $\sqrt{\alpha t}$, giving a length 0.0028 m for $\alpha_{air} = 2E-5\,m^2/s$ and $t = 0.4\,s$. A similar flow was simulated by Pericleous et al. [14]. It was found that the thermal layer in their results is quite thick. One reason for this is the coarse grid adopted in their calculations. However, a most important factor is the diffused-layer method used by them. It could be identified from their contour plots of VOF function that the interface is greatly smeared. As a result, the thermal layer around the interface is also diffused.

Falling of a Liquid Tin Droplet in Oil

A square tank of 0.008 m is filled with oil at temperature 250°C. A 2-D molten tin droplet of size 0.002 m in diameter and temperature 800°C is released. The initial

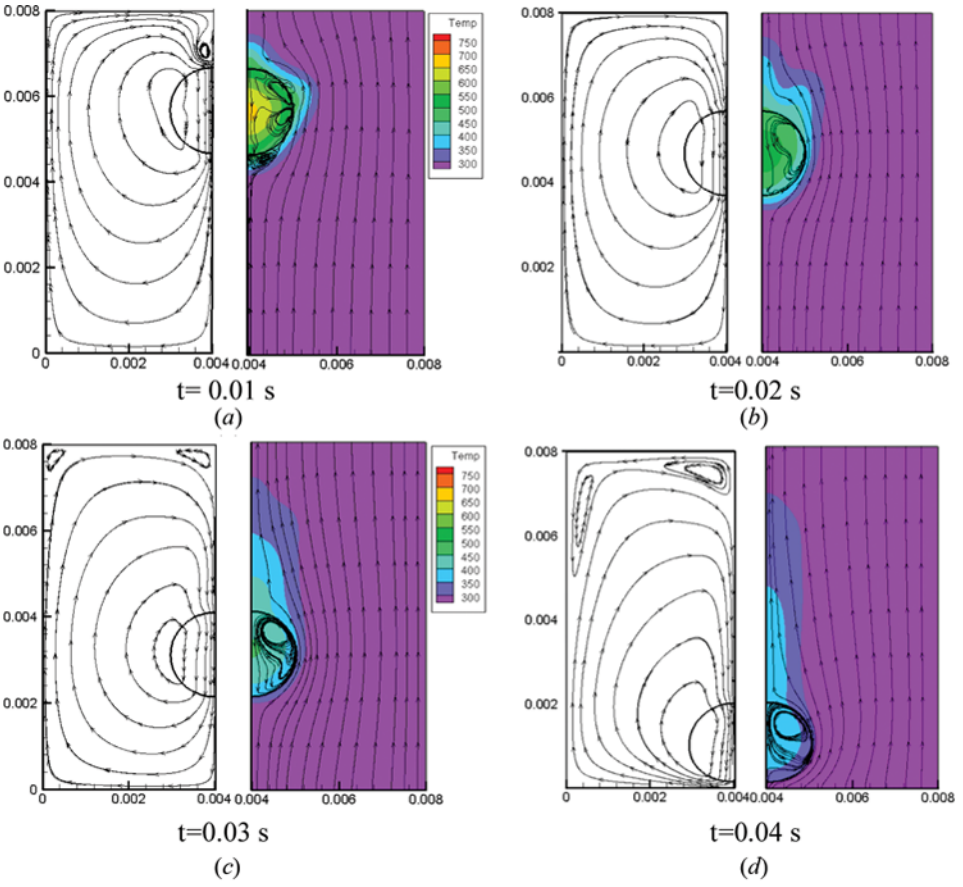

Figure 12. Flow and temperature fields for the case with zero initial velocity. The streamlines on the left are on the laboratory frame and those on the right are on the relative frame.

velocity is assumed to be 0 or 0.5 m/s. The walls surrounding the tank are insulated. The grid size for computation is 2.2×10^{-5} m. The thermodynamic properties are $\rho = 6{,}970\,\mathrm{kg/m^3}$, $C_P = 244\,\mathrm{J/kg\,K}$, $k = 33.6\,\mathrm{W/m\,K}$, and $\mu = 1.92 \times 10^{-3}\,\mathrm{N\,s/m^2}$ for the molten tin, and $\rho = 1{,}067\,\mathrm{kg/m^3}$, $C_P = 2{,}700\,\mathrm{J/kg\,K}$, $k = 22.6\,\mathrm{W/m\,K}$, and $\mu = 2.28 \times 10^{-3}\,\mathrm{N\,s/m^2}$ for the oil. The surface tension coefficient is given by $\sigma = 0.5\,\mathrm{N/m}$.

As shown in Figure 11 for the zero-initial-velocity case, the falling speed of the droplet, characterized by that at the droplet center along the center axis, is accelerated in a linear manner until it is very close to the bottom wall, where the maximum speed is about 0.23 m/s. Owing to the low velocity, the geometry of the droplet remains nearly a circle except when it approaches the bottom wall. The streamlines shown on the left of each sketch in Figure 12 indicate that the flow field in the tank is dominated by a vertical vortex induced by the falling droplet. In order to illustrate the effect of convection on heat transfer, the flow field is transformed onto a frame of reference relative to the moving bubble, obtained via subtracting the droplet velocity from the velocity field. The streamlines on this relative frame are presented on the right of each sketch in the figure. It can be seen that a recirculation zone is found at the stagnation region on the front side of the droplet and a small separation bubble at the rear side at the early time $t = 0.01$ s. Beyond the early stage, the oil flows smoothly over the droplet. Flow recirculation develops and becomes dominant inside the droplet. When the droplet is close to the bottom, streamlines penetrate into the droplet. It is obvious that the temperature distribution is closely related to the flow pattern. The oil flowing over the droplet carries away the thermal energy of the molten droplet, resulting in the temperature contours shown in the figure.

The falling speed of the droplet is given in Figure 13 for the case with initial velocity 0.5 m/s. It is decelerated first, followed by acceleration. The minimum speed

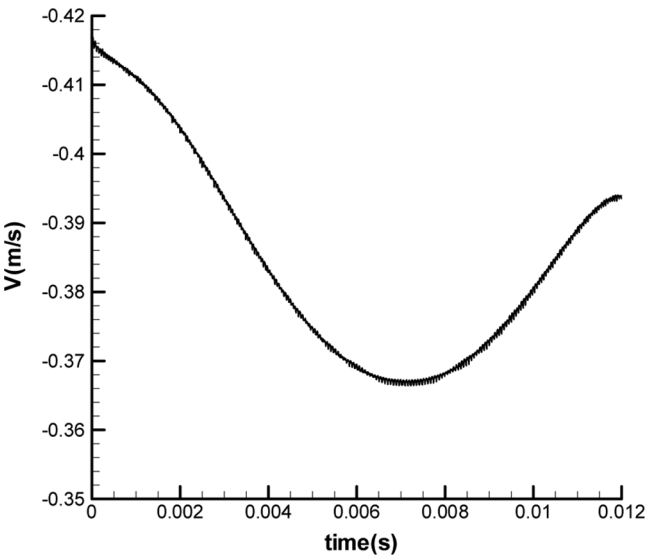

Figure 13. Variation of droplet speed for the case with initial velocity 0.5 m/s.

occurs at 0.007 s. The droplet changes its shape constantly during this process, as seen from Figure 14. The convex side faces the bottom wall in the decelerating stage and changes its facing direction toward the upper wall in the accelerating stage. At $t = 0.007$ s, the droplet is in a shape of ellipse. To illustrate the cause of the droplet geometry change, pressure contours are presented in Figure 15 for $t = 0.005$ and 0.009 s, respectively representing the decelerating and accelerating stages. It is clear that the core pressure inside the droplet is much higher than the pressure outside. Comparing the lower surface (the front side of the falling droplet), the pressure on the upper surface (the rear side) of the droplet is always lower throughout the entire process. However, it can be found by closely examining the pressure distribution around the surface of the droplet that the pressure difference across this interface on the upper side is smaller than that on the lower side at $t = 0.005$ s, whereas the situation on the two side surfaces is reversed for $t = 0.009$ s. According to the Young-Laplace equation, the pressure difference across the interface is

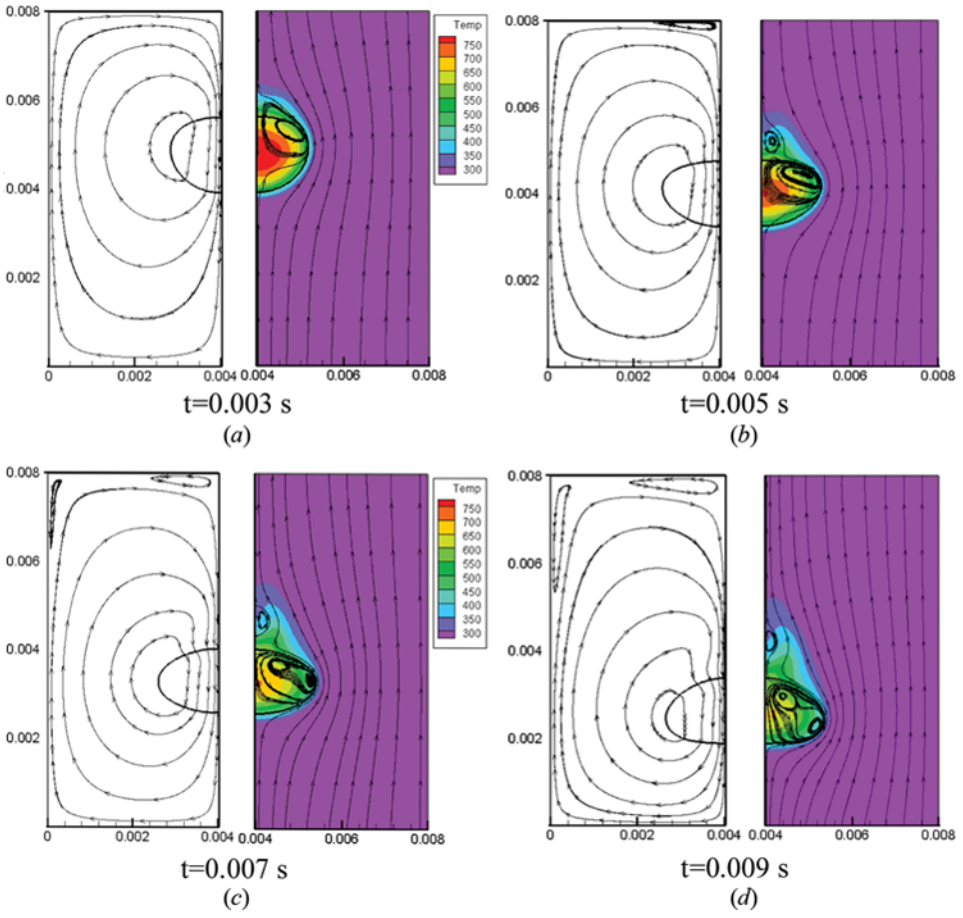

Figure 14. Flow and temperature fields for the case with initial velocity 0.5 m/s. The streamlines on the left are on the laboratory frame and those on the right are on the relative frame.

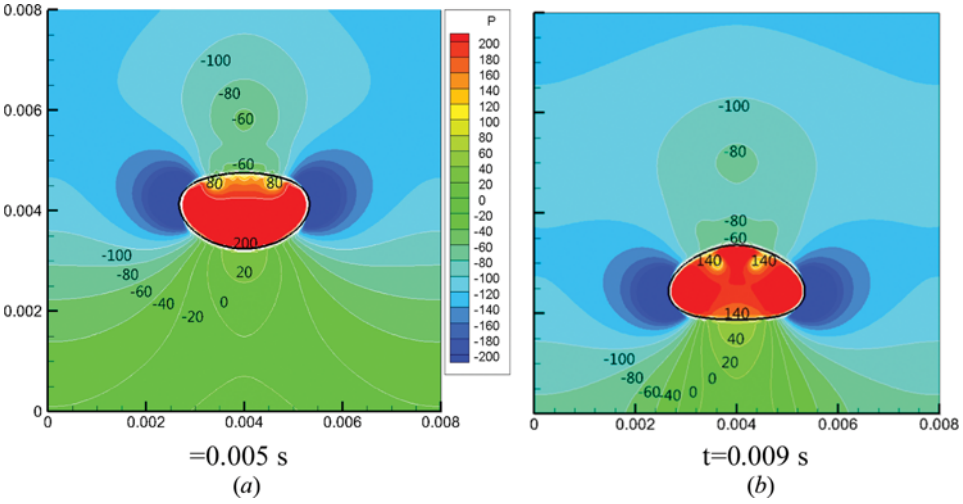

Figure 15. Pressure distribution for the case with initial velocity 0.5 m/s.

balanced by the surface tension, which is linearly related to the surface curvature. Therefore, it is not surprising to get flatter surface on the upper side during the decelerating period and on the lower side when the droplet is accelerated.

It is seen from Figure 14 that the streamlines on the relative frame penetrate into the droplet and recirculating flow is developed in the droplet at $t = 0.003$ s. The coverage of the recirculation zone extends beyond the droplet. The recirculation is then transformed into two vortices, as seen at $t = 0.005$ s. A bigger one remains in the droplet and a small one is formed in the wake just downstream of the droplet. The vortex in the wake moves away from the droplet, and its size is gradually decreased in the latter time. The flow inside the droplet is complicated, with smaller vortices developed and embedded in the big one. The streamline penetration ends as time approaches 0.005 s. The effect of the vortex flow on heat transfer in the wake is quite obvious by noting that the temperature contours are bent backward in this region.

CONCLUDING REMARKS

A sharp-interface model to tackle heat transfer across the interface between two immiscible fluids has been developed. It is based on satisfaction of the continuity condition to find temperature and heat flux at the interface. The temperature at relevant locations in the interface cell can then be calculated using the interface temperature, which is imposed as internal boundary condition for energy solution.

In the model testing cases, heat conduction in two solids, being in contact, was considered. In one case, the initial temperature is continuous at the contact surface. The calculation shows good agreement with the exact solution. In the other case, a jump in the initial temperature exists between the two solids. There is no theoretical solution available, but a reference solution is derived, which is used for quantitative assessment of the method. It is seen that the numerical results follow the trend of the reference solution closely.

In flow applications, heat transfer from collapse of a heated water column in a cavity was first examined. The mechanism of heat transfer in this flow is mainly due to thermal conduction. A thin thermal layer can be found in the interface region, demonstrating that numerical diffusion can be waived by using this model. The second flow case was to consider a 2-D molten tin droplet falling into an oil tank. To illustrate flow effect on the heat transfer, the velocity field is transformed onto a relative frame of reference. It was shown that strong recirculating flow is formed in the droplet. A small recirculation zone appears in the wake of the droplet for the case with initial velocity 0.5 m/s. Thermal energy is carried away by the oil flowing over the droplet. The dependence of the temperature contour on the flow pattern is clearly identified.

FUNDING

This work was supported by the National Science Council of the Republic of China under Contract Numbers NSC 101-2221-E009-044 and NSC 102-2221-E009-059.

REFERENCES

1. Y. Ohno, The Latest Molten Metal Refining Progress in Cast Shop, *J. Japan Inst. Light Metals*, vol. 51, pp. 134–37, 2001.
2. J. Mitrovic and K. Stephan, Mean Fluid Temperatures in Direct Contact Heat Exchangers without Phase Change, *Int. J. Heat Mass Transfer*, vol. 39, pp. 2745–2750, 1996.
3. M. R. Barkhudarov, Is Fluid Flow Important for Predicting Solidification?, Solidification Processing '97 Conference, July 1997, Sheffield, UK.
4. J.-F. Hetu and F. Ilinca, A Finite Element Method for Casting Simulations, *Numer. Heat Transfer A*, vol. 36, pp. 657–679, 1999.
5. K. Park, A Study on Flow Simulation and Deformation Analysis for Injection-Molded Plastic Parts Using Three-Dimensional Solid Elements, *Polymer-Plastics Tech. Eng.*, vol. 43, pp. 1569–1584, 2004.
6. W. J. Rider and D. B. Kothe, Reconstructing Volume Tracking, *J. Comput. Phys.*, vol. 141, pp. 112–152, 1998.
7. O. Ubbink and R. I. Issa, A Method for Capturing Sharp Fluid Interfaces on Arbitrary Meshes, *J. Comput. Phys.*, vol. 153, pp. 26–50, 1999.
8. Y.-Y. Tsui, S.-W. Lin, T.-T. Cheng, and T.-C. Wu, Flux-Blending Schemes for Interface Capture in Two-Fluid Flows, *Int. J. Heat Mass Transfer*, vol. 52, pp. 5547–5556, 2009.
9. M. Sussman, E. Fatami, P. Smereka, and S. Osher, An Improved Level Set Method for Incompressible Two-Phase Flows, *Comput. Fluids*, vol. 27, pp. 663–680, 1998.
10. S. Osher, Level Set Method: An Overview and Some Recent Results, *J. Comput. Phys.*, vol. 79, pp. 12–49, 2001.
11. C. S. Peskin, Numerical Analysis of Blood Flow in the Heart, *J. Comput. Phys.*, vol. 25, pp. 220–252, 1977.
12. J. J. Monaghan, Simulating Free Surface Flow with SPH, *J. Comput. Phys.*, vol. 110, pp. 399–406, 1994.
13. G. J. Storr and M. Behnia, Comparisons between Experiment and Numerical Simulation Using a Free Surface Technique of Free-Falling Liquid Jets, *Exp. Thermal Fluid Sci.*, vol. 22, pp. 79–91, 2000.

14. K. A. Pericleous, K. S. Chan, and M. Cross, Free Surface Flow and Heat Transfer in Cavities: The SEA Algorithm, *Numer. Heat Transfer B*, vol. 27, pp. 487–507, 1995.
15. B. van Leer, Towards the Ultimate Conservative Difference Scheme IV: A New Approach to Numerical Convection, *J. Comput. Phys.*, vol. 23, pp. 276–299, 1977.
16. V. Mehdi-Nejad, J. Mostaghimi, and S. Chandra, Modelling Heat Transfer in Two-Fluid Interfacial Flows, *Int. J. Numer. Meth. Eng.*, vol. 61, pp. 1028–1048, 2004.
17. M. R. Davidson and M. Rudman, Volume-of-Fluid Calculation of Heat or Mass Transfer across Deforming Interfaces in Two-Fluid Flow, *Numer. Heat Transfer B*, vol. 41, pp. 291–308, 2002.
18. S. T. Zalesak, Fully Multidimensional Flux-Corrected Transport Algorithms for Fluids, *J. Comput. Phys.*, vol. 31, pp. 335–262, 1979.
19. A. Esmaeeli and G. Tryggvason, Computations of Film Boiling Part I: Numerical Method, *Int. J. Heat Mass Transfer*, vol. 47, pp. 5451–5461, 2004.
20. S. W. J. Welch and J. Wilson, A Volume of Fluid Based Method for Fluid Flows with Phase Change, *J. Comput. Phys.*, vol. 160, pp. 662–682, 2000.
21. Y.-Y. Tsui, S.-W. Lin, Y.-N. Lai, and F.-C. Wu, Phase Change Calculations for Film Boiling Flows, *Int. J. Heat Mass Transfer*, vol. 70, pp. 745–757, 2014.
22. J. U. Brackbill, D. B. Kothe, and C. Zemach, A Continuum Method for Modeling Surface Tension, *J. Comput. Phys.*, vol. 100, pp. 335–354, 1992.
23. Y.-Y. Tsui and S.-W. Lin, A VOF Based Conservative Interpolation Scheme for Interface Tracking (CISIT) of Two-Fluid Flows, *Numer. Heat Transfer B*, vol. 63, pp. 263–283, 2013.
24. Y.-Y. Tsui and Y.-F. Pan, A Pressure-Correction Method for Incompressible Flows Using Unstructured Meshes, *Numer. Heat Transfer B*, vol. 49, pp. 43–65, 2006.
25. Y.-Y Tsui and T.-C. Wu, A Pressure-Based Unstructured-Grid Algorithm Using High Resolution Schemes for All-Speed Flows, *Numer. Heat Transfer B*, vol. 53, pp. 75–96, 2008.
26. Y.-Y. Tsui, Y.-C. Huang, C.-L. Huang, and S.-W. Lin, A Finite-Volume Based Approach for Dynamic Fluid-Structure Interaction, *Numer. Heat Transfer B*, vol. 64, pp. 326–349, 2013.
27. V. S. Arpaci, *Conduction Heat Transfer*, Addison-Wesley, Reading, MA, 1966.